Manuscript prepared for Clim. Past Discuss.
with version 2014/07/29 7.12 Copernicus papers of the LaTeX class copernicus.cls.
Date: 5 January 2015

Early deglacial Atlantic overturning decline and its role for atmospheric CO_2 rise inferred from carbon isotopes ($\delta^{13}C$)

A. Schmittner[1] **and D. C. Lund**[2]

[1]College of Earth, Ocean, and Atmospheric Sciences, Oregon State University, Corvallis, Oregon, USA
[2]Department of Marine Sciences, University of Connecticut, USA

Correspondence to: A. Schmittner (aschmitt@coas.oregonstate.edu)

Discussion Paper | Discussion Paper | Discussion Paper | Discussion Paper |

Abstract

The reason for the initial rise of atmospheric CO_2 during the last deglaciation remains unknown. Most recent hypotheses invoke Southern Hemisphere processes such as shifts in mid-latitude westerly winds. Coeval changes in the Atlantic Meridional Overturning Circulation (AMOC) remain poorly quantified and their relation to the CO_2 increase is not understood. Here we compare simulations from a global, coupled climate-biogeochemistry model that includes a detailed representation of stable carbon isotopes ($\delta^{13}C$) with a synthesis of high-resolution $\delta^{13}C$ reconstructions from deep sea sediments and ice core data. In response to a prolonged AMOC shutdown initialized from a pre-industrial state, modeled $\delta^{13}C$ of Dissolved Inorganic Carbon ($\delta^{13}C_{DIC}$) decreases in most of the surface ocean and the subsurface Atlantic, with largest amplitudes (more than 1.5‰) in the intermediate depth North Atlantic. It increases in the intermediate and abyssal South Atlantic, as well as in the subsurface Southern, Indian and Pacific oceans. The modeled pattern is similar and highly correlated with the available foraminiferal $\delta^{13}C$ data spanning the late Last Glacial Maximum (LGM, $\sim$19.5–18.5 ka BP) to the late Heinrich Stadial Event 1 (HS1, $\sim$16.5–15.5 ka BP), but the model overestimates $\delta^{13}C_{DIC}$ reductions in the North Atlantic. Possible reasons for the model-sediment data differences are discussed. Changes in remineralized $\delta^{13}C_{DIC}$ dominate the total $\delta^{13}C_{DIC}$ variations in the model but preformed contributions are not negligible. Simulated changes in atmospheric CO_2 and its isotopic composition ($\delta^{13}C_{CO_2}$) agree well with ice core data. Modeled effects of AMOC induced wind changes on the carbon and isotope cycles are small, suggesting that Southern Hemisphere westerly wind effects may have been less important for the global carbon cycle response during HS1 than previously thought. Our results indicate that during the early deglaciation the AMOC decreased for several thousand years. We propose that the observed early deglacial rise in atmospheric CO_2 and the decrease in $\delta^{13}C_{CO_2}$ may have been dominated by an AMOC induced decline of the ocean's biologically sequestered carbon storage.

1 Introduction

Earth's transition from the LGM (23–19 ka BP; thousand years before the present), into the modern warm period of the Holocene (10–0 ka BP) remains enigmatic (Denton et al., 2006). Evidence of early warming of the Southern Hemisphere and atmospheric CO_2 increase (Petit et al., 1999; Denton et al., 2010) has prompted hypotheses of a Southern Hemisphere trigger for the deglaciation (Stott et al., 2007; Timmermann et al., 2009). But the early rise in atmospheric CO_2, although an important forcing for deglacial global warming (Shakun et al., 2012), remains unexplained. Various mechanisms have been proposed. Prominent recent studies suggest wind (Anderson et al., 2009; Denton et al., 2010; Toggweiler et al., 2006) and/or stratification (Watson and Naveira Garrabato 2006; Schmittner et al. 2007; Sigman et al. 2007; Tschumi et al., 2011) changes in the Southern Ocean and/or changes in the North Pacific circulation (Menviel et al., 2014).

Others have suggested that the deglaciation was initiated by a collapse of the AMOC caused by melting of Northern Hemisphere ice sheets (Clark et al., 2004; Sigman et al. 2007; Anderson et al., 2009; Denton et al., 2010; Shakun et al., 2012; He et al., 2013) and abrupt North Atlantic climate changes (Broecker et al., 1985). This idea has appeal since the AMOC is known from theory to exhibit multiple steady states with the possibility of rapid transitions between them (Stommel, 1961). Moreover, AMOC variations are consistent with the observed antiphasing of surface temperatures between the hemispheres (Crowley 1992; Blunier et al., 1998; Schmittner et al., 2003; Stocker and Johnson, 2003; EPICA community members 2006; Shakun et al., 2012) and evidence for ITCZ migration (Menviel et al., 2008). However, surface temperatures and tropical rainfall patterns alone do not allow robust inferences on the AMOC (Kurahashi-Nakamura et al., 2014) and evidence from the deep ocean for circulation variations remains sparse. One widely cited record of Protactinium-Thorium ratios ($^{231}Pa/^{230}Th$) from the subtropical North Atlantic has been interpreted as AMOC collapse around 19–18 ka BP followed by a rapid resumption ~ 15 ka BP into the warm Boelling/Allerod period (McManus et al., 2004). However, this interpretation has been questioned (Keigwin and Boyle, 2008) and a subsequent set of

$^{231}Pa/^{320}Th$ records (Gherardi et al., 2009) suggested that a complete AMOC cessation during HS1 was unlikely. Moreover, our understanding of $^{231}Pa/^{230}Th$ in the modern ocean continues to evolve (Anderson and Hayes, 2013) and inferences on the basin or global scale circulation from a single site require validation with multiple proxies from a range of oceanographic locations. A quantitative deglacial AMOC reconstruction constrained by distributed interior ocean observations remains lacking. Here we attempt a first step towards such a reconstruction by combining model simulations with $\delta^{13}C$ measurements of sediment samples.

Deep sea reconstructions based on $\delta^{13}C$ are more common than $^{231}Pa/^{230}Th$, the processes governing $\delta^{13}C$ are better understood, and realistic three-dimensional models exist (e.g. Schmittner et al., 2013), providing necessary ingredients for quantitative hypothesis testing. Here we compile deep ocean $\delta^{13}C$ reconstructions at high temporal resolution from the early deglaciation and compare them with model simulations of $\delta^{13}C$ changes caused by AMOC variations in order to test the hypothesis that the AMOC was reduced during HS1. We also compare our model results to observations of atmospheric CO_2 concentrations and its $\delta^{13}C$ values in order to assess mechanisms of the early deglacial CO_2 rise. Here we do not address the full deglaciation but restrict our investigation to its initial phase from the late LGM ($\sim$19.5–18.5 ka BP) to the late HS1 ($\sim$16.5–15.5 ka BP).

Various modeling studies have previously examined the effect of AMOC changes on atmospheric CO_2, with sometimes conflicting results (Marchal et al., 1998; Marchal et al., 1999; Scholze et al., 2003; Köhler et al., 2005; Schmittner et al., 2007a; Obata, 2007; Schmittner and Galbraith, 2008; Menviel et al., 2008, 2012, 2014; Bozbiyik et al., 2011). Schmittner and Galbraith (2008) found that a large AMOC reduction decreases the efficiency of the ocean's biological pump if North Atlantic Deep Water (NADW) is more depleted in preformed nutrients than southern sourced water masses (Antarctic Bottom Water (AABW) and Antarctic Intermediate Water (AAIW)) and thus leads to outgassing of CO_2 into the atmosphere and gradually increasing atmospheric CO_2 over several thousand years, consistent with theory (Ito and Follows 2005; Marinov et al., 2008a, b) and ice core CO_2 reconstructions (Ahn and Brook, 2007). Some of the differences in model responses may

thus be due to the simulations of preformed nutrients. Whereas Schmittner and Galbraith (2008) have demonstrated consistency of their model with modern preformed nutrient observations such a validation is not published, to our knowledge, for other models (e.g. the LOVECLIM model used by Menviel et al., 2008, 2014). Several studies found dependency of the results on the initial state (Köhler et al., 2005; Schmittner et al., 2007a; Menviel et al., 2008) suggesting that starting from glacial conditions may give a different answer than starting from modern conditions. However, none of these studies have validated their initial deep ocean LGM states with reconstructions. Thus inferences from these studies regarding the sensitivity of the real ocean carbon cycle to initial conditions remain subject to considerable uncertainty.

Effects of southern hemisphere westerly winds on atmospheric CO_2 have also been quantified with models before (Winguth et al., 1999, Menviel et al., 2008, Tschumi et al., 2008, 2011, d'Orgeville et al., 2010, Lee et al., 2011, Völker and Köhler, 2013). Most of these studies conclude that reasonably expected changes in the strength and/or latitude of westerly winds cannot explain a large fraction of the observed 100 ppm glacial-interglacial CO_2 amplitude (Winguth et al., 1999, Menviel et al., 2008, Tschumi et al., 2008, 2011, d'Orgeville et al., 2010, Völker and Köhler, 2013). An exception is the work by Lee et al. (2011), who find a 20 - 60 ppm CO_2 increase for a 25% strengthening of the westerly winds. However, their wind stress forcing was calculated from an atmosphere only model, which was forced with a very large heat flux anomaly and leads to large areas of the subtropical North Atlantic experiencing extreme cooling of more than 10°C, much more than reconstructed (Bard et al., 2000). We will show below that more realistic coupled ocean-atmosphere model simulations of an AMOC collapse result in much smaller wind stress changes. For comparison, a complete removal of the Antarctic Ice Sheet leads only to a 50% reduction in southern hemisphere westerly winds (Schmittner et al., 2011). Tschumi et al. (2011), who's simulations include $\delta^{13}C$ and are forced with wind stress changes over the Southern Ocean, conclude that stratification changes there can explain the observed rise of atmospheric CO_2 and the decrease in $\delta^{13}C_{CO2}$ during HS1. Here we propose a different mechanism, namely changes in the AMOC and its effect on the efficiency of the

biological pump, as an alternative hypothesis for the ice core observations. Another difference from previous studies is that we directly and quantitatively test Anderson et al.'s (2009) hypothesis that AMOC changes affect atmospheric circulation and wind stress in the Southern Ocean to such a degree that outgassing of CO_2 contributes importantly to the total CO_2 rise during HS1. We do this by applying realistic wind stress changes from a coupled ocean-atmosphere model simulation of an AMOC shutdown to a global carbon cycle model including isotopes.

2 Methods

We have compiled 25 published deep ocean records covering the early deglaciation at high temporal resolution (Table 1). Mostly published age models are used, except in some cases where the radiocarbon calibration was updated as described in Lund et al. (2014). In order to be consistent with the treatment of the other cores in Lund et al. (2014) we have updated the age model of MD01-2461 by recalibrating the radiocarbon ages using INTCAL13 and reservoir ages estimated by Stern and Lisiecki (2013). The ages may have considerable (O(1 ka)) uncertainties. However, we believe that the records are of sufficient resolution and their age models are well enough constrained to evaluate multi-millennial changes. The purpose of this paper is to present an initial comparison to model results focusing on model analysis. Quantification of age uncertainties and their effects on the results are beyond the scope of this paper. The sediment data compilation is available in the supplement to this paper.

We employ the Model of Ocean Biogeochemistry and Isotopes (MOBI 1.4), a coupled climate-biogeochemical system that includes $\delta^{13}C$ cycling in the three-dimensional ocean, land, and atmosphere to explore the effect of AMOC variations on carbon isotopes (see appendix for a more detailed model description). MOBI's large-scale ocean distribution of $\delta^{13}C_{DIC}$ in dissolved inorganic carbon (DIC) is consistent with modern water column observations (Schmittner et al., 2013). It is embedded in the University of Victoria climate model of intermediate complexity version 2.9 and run into a *pre-industrial* equilib-

rium with prognostic atmospheric CO_2 and $\delta^{13}C_{CO_2}$. Subsequently four numerical experiments, each ~ 3500 years long, have been conducted with varying amplitudes (0.05 Sv, 0.1 Sv, 0.15 Sv, and 0.2 Sv; referred to as FW0.05, FW0.1, FW0.15, and FW0.2, respectively; Sv = Sverdrup = 10^6 m^3 s^{-1}). In each case we apply a stepwise, 400 year long freshwater input to the North Atlantic between 45-65°N and 60-0°W (Fig. 1a). The added freshwater is not compensated elsewhere but it affects surface tracer concentrations though dilution. Lower salinity and increased buoyancy of surface waters causes the AMOC to slow down. Note that these are idealized experiments, designed to examine only how AMOC variations impact the global $\delta^{13}C$ distribution. Realistic initial conditions for the LGM are currently not available. Thus, we do not attempt realistic deglacial simulations. However, it is well known that the $\delta^{13}C$ distribution of the LGM ocean (Curry and Oppo, 2005; Gebbie, 2014) and atmospheric CO_2 concentrations (Monnin et al., 2001; Lourantou et al., 2010; Parrenin et al., 2013; Marcott et al., 2014) were different from the pre-industrial. In order to account for these differences in initial conditions our data-model comparison focuses on anomalies rather than absolute values. Possible sensitivity of the results on initial conditions is further discussed in the discussion section below. Selected model data are available in the supplement to this paper.

3 Results

3.1 Simulated circulation changes

The AMOC reduces in all experiments (Fig. 1b). However, in FW0.05 and FW0.1 the reduction is reversible and after hosing is stopped the AMOC quickly returns to its initial state. In experiments FW0.15 and FW0.2, on the other hand, the AMOC collapses permanently (Fig. 2). Reduced salt input to the deep ocean by North Atlantic Deep Water (NADW) leads to freshening of the deep ocean and salinification of the surface (not shown here; see Figs. 5, 6 and Plate 2 in Schmittner et al., 2007a), deeper mixed layers and decreased stratifica-

tion in the Southern Ocean (Schmittner et al., 2007a) and North Pacific (Saenko et al., 2005) as illustrated in Fig. 2 by the thickening of isopycnal layers between $26.8 \leq \sigma_\Theta \leq 27.63$.

3.2 Simulated carbon cycle changes

The effect on atmospheric CO_2 in model simulations with partial and short AMOC reductions (FW0.05 and FW0.1) is negligible. In contrast, in the simulations with a large and prolonged AMOC decline (FW0.15 and FW0.2) CO_2 starts to rise about 500 years after the beginning of the hosing. It continues to increase gradually by ~ 25 ppm until year 2000, after which its rate of change slows. The amplitude and rate of change of the simulated CO_2 increase agrees well with the long term trend of measurements of HS1 air recovered from Antarctic ice (Monin et al., 2011; Parrenin et al., 2013; Marcott et al., 2014), but the model does not reproduce the rapid increase around year 16,250 BP.

The simulated atmospheric CO_2 increase in FW0.15 and FW0.2 is due to a loss of ocean carbon to the atmosphere. Initially Net Primary Production (NPP) declines within a few hundred years from 64 Pg C yr^{-1} to 54 Pg C yr^{-1} consistent with Schmittner (2005; not shown here), which reduces the production of dissolved organic carbon (DOC), whereas dissolved inorganic carbon increases initially until around year 600, after which it starts to decline. By model year 3500 the ocean has lost ~ 120 Pg C (Fig. 3d) in FW0.15 most of which (~ 90 Pg C) due to DIC, and less (~ 30 Pg C) due to DOC. The ocean's DIC loss is caused by a reduced efficiency of the biological pump as indicated by the large loss of remineralized DIC (~ 400 Pg C; Fig. 3g) most of which is due to less organic matter oxidation (DIC_{org}; Fig. 4), whereas it is buffered by the increase in preformed DIC due to rising surface ocean DIC and atmospheric CO_2 consistent with previous results and theory (Schmittner and Galbraith, 2008; Ito and Follows, 2005; Marinov et al., 2008a, b).

3.3 Simulated carbon isotope changes

The loss of biologically sequestered, isotopically light ($\delta^{13}C_{org} = -20‰$) organic carbon increases deep ocean $\delta^{13}C_{DIC}$ by $\sim 0.06‰$ (Fig. 3f). Accumulation of this isotopically light

carbon in the surface ocean and atmosphere decreases their $\delta^{13}C_{DIC}$ (by ~ -0.3 ‰) and $\delta^{13}C_{CO_2}$ by ~ -0.25 ‰, respectively (Fig. 1d). Modeled land carbon storage increases (Fig. 3a) and its average $\delta^{13}C_L$ decreases (Fig. 3c), implying that land cannot be the cause of the atmospheric changes. The simulated atmospheric $\delta^{13}C_{CO_2}$ decline in models FW0.15 and FW0.2 is consistent, both in amplitude and rate of change, with ice core measurements (Fig. 1d; Schmitt et al., 2012) but the model response may depend on boundary and/or initial conditions and this agreement may be fortuitous.

The simulated pre-industrial (model year 0; Fig. 5a–c) distribution of $\delta^{13}C_{DIC}$ in the ocean is characterized by high values in the surface and deep North Atlantic and low values in the deep North Pacific, consistent with a previous model version and observations (Schmittner et al., 2013). Sinking of isotopically well equilibrated surface waters with low nutrient and respired carbon content causes high $\delta^{13}C_{DIC}$ values in the deep North Atlantic, whereas aging and accumulation of isotopically light respired organic matter progressively decreases $\delta^{13}C_{DIC}$ as deep waters flow into the South Atlantic, and further into the Indian and Pacific Oceans. Thus, the modern inter-basin difference in deep water $\delta^{13}C_{DIC}$ is caused by the interbasin MOC (Boyle and Keigwin, 1982). Hence, as the AMOC collapses, the $\delta^{13}C_{DIC}$ difference between North Atlantic and North Pacific deep waters is reduced (Fig. 5d–f).

Differences between years 2500 and 0 (Fig. 5g–i) show the largest $\delta^{13}C_{DIC}$ decreases at intermediate depths (1–2.5 km) in the northern North Atlantic. Anomalies decrease further south but a pronounced minimum emerges at the depth of NADW (2–3 km, Fig. 2) in the South Atlantic with positive anomalies below, at the depth of Antarctic Bottom Water, and above, at the depth of Antarctic Intermediate Water. South of 40° S in the Atlantic as well as in the Indian and Pacific oceans $\delta^{13}C_{DIC}$ increases everywhere below ~ 500 m due to reduced export of ^{13}C-depleted carbon from the photic zone. Weakening of the biological pump causes surface ocean $\delta^{13}C$ to decrease by 0.2–0.4 ‰ in the Indian and Pacific basins, possibly explaining the onset of planktonic $\delta^{13}C$ minima on glacial terminations (Spero and Lea, 2002). The deep ocean signal dominates the global mean $\delta^{13}C_{DIC}$ increase of 0.04 ‰ by year 2500 (Fig. 3f). In the North Pacific $\delta^{13}C_{DIC}$ shows the largest increase around 1 km depth owing to reduced stratification and intensified intermediate water formation (Saenko

et al., 2005), which decreases the amount of respired carbon and increases remineralized $\delta^{13}C$ ($\delta^{13}C_{rem}$; Fig. 6) there. $\delta^{13}C_{rem}$ increases in most of the deep Pacific, Indian and Southern oceans due to the loss of respired carbon, whereas in the Atlantic respired carbon accumulates leading to a decrease in $\delta^{13}C_{rem}$. Although changes in $\delta^{13}C_{rem}$ dominate the spatial variations of the total $\delta^{13}C_{DIC}$ changes, preformed $\delta^{13}C$ ($\delta^{13}C_{pre}$) variations are not negligible, particularly in the Atlantic, where they decrease by more than 0.3 ‰.

3.4 Observed carbon isotope changes during HS1

Observations from the North Atlantic show large $\delta^{13}C_{DIC}$ decreases early in the deglaciation (Fig. 7a–e; Fig. 8a). The largest amplitudes (~ 1 ‰) are found in high-resolution records from the northern North Atlantic (61° N) at intermediate (1.3–1.6 km) depths (Praetorius et al., 2008; Rickaby and Elderfield, 2005; Thornalley et al., 2010). Further south and in deeper water the $\delta^{13}C_{DIC}$ decrease is smaller (0.4 to 0.7 ‰) (Vidal et al., 1997; Hodell et al., 2010; Zahn et al., 1997; Skinner and Shackleton, 2004; Labeyrie et al., 2005; Zahn and Stuber, 2002). Changes simulated at the same locations by model experiments FW0.15 and FW0.2, which exhibit multi-millennial AMOC collapses, are generally similar in amplitude, albeit somewhat larger and in some cases earlier. Note that the timing of the rapid $\delta^{13}C_{DIC}$ decrease in core NEAP4K is later than in the two nearby cores ODP984 and RAPID-10-1P, presumably because the age model of NEAP4K is not as well constrained as those from the other two cores.

Despite similar AMOC evolutions model FW0.15 shows smaller amplitudes than model FW0.2, in better agreement with the reconstructions, due to local effects of the different freshwater forcing on stratification and $\delta^{13}C_{DIC}$. The overall spatial distribution of the observed $\delta^{13}C_{DIC}$ changes, with largest amplitudes at intermediate depths in the northern North Atlantic and decreasing further south and in deeper waters, is in best agreement with the results from model FW0.15 (Figs. 7 and 8; Table 2).

A new dataset from the Brazil Margin in the South Atlantic (Fig. 7f–k; Fig. 9) (Tessin and Lund, 2013; Lund et al., in review) shows increasing $\delta^{13}C_{DIC}$ by $0.2-0.4$ ‰ between 1.1 and 1.3 km depth and decreasing $\delta^{13}C_{DIC}$ by ~ 0.5 ‰ between 1.6 and 2.1 km depth, whereas

deeper in the water column the data are noisier without a clear trend. Model FW0.15's initial $\delta^{13}C_{DIC}$ values at the Brazil Margin are higher than the observations' mainly for two reasons (Fig. 9). First, the model does not consider the whole ocean lowering of $\delta^{13}C_{DIC}$ due to the reduction in land carbon during the LGM and second, it does not include the shoaling of NADW and very low $\delta^{13}C_{DIC}$ values in South Atlantic bottom waters (Curry and Oppo, 2005; Gebbie, 2014). Thus the simulated $\delta^{13}C_{DIC}$ decrease extends deeper than in the observations and shows a substantial reduction below 2.2 km. However, the reconstructed pattern of opposing $\delta^{13}C$ signal between shallow-intermediate and mid-depths agrees well with the simulated changes due to large AMOC reduction (Fig. 9). The rapid initial increase at intermediate depths appears to be influenced by two factors. First, there is reduced return flow of low $\delta^{13}C_{DIC}$ from the Indian ocean (not shown). Second, less upwelling (Schmittner et al., 2005) of low $\delta^{13}C_{DIC}$ deep water into the upper and surface Southern Ocean leads to a deepening of the high $\delta^{13}C_{DIC}$ Antarctic Intermediate and Subantarctic Mode Waters, which, together with decreased stratification and deeper mixed layers (Schmittner et al., 2007a; Fig. 2), increases $\delta^{13}C_{DIC}$ by ~ 0.3 ‰ at 1.2 km depth in all ocean basins at mid southern latitudes (Fig. 5g–i).

The simulated $\delta^{13}C_{DIC}$ increase at 1.2 km depth in the southwest Pacific (~ 0.5 ‰) and at 1.6 km depth in the tropical Indian Ocean (~ 0.3 ‰) agree well with local reconstructions (Fig. 7p and o), but the simulated changes happen 1.5 ka earlier than in the sediment data. The lack of age model error estimates for the sediment data currently prevents a more detailed assessment of the simulated temporal evolution. In deep waters of the Southern and Indian Oceans the reconstructions are noisy and no clear trend can be identified (Fig. 7l–n). Core W8709A-13PC from the deep eastern North Pacific (Lund et al. 2011) shows no trend in contrast to models FW0.15 and FW0.2. More data from the deep North Pacific are needed in order to better assess model simulations there.

3.5 Sensitivity to wind changes

The model results discussed above did not include the effects of wind changes. Winds enter the UVic model in three ways:

1. Moisture advection velocities u_q determine convergence of specific humidity and thus precipitation.

2. Wind stress τ supplies momentum to the surface ocean and sea ice.

3. Wind speed u modulates air–sea exchange of heat, water, and gases (CO_2, O_2).

Fig. 11 shows the annual mean fields derived from the NCEP reanalysis (Kalnay et al., 1996) used in the above runs.

In order to test the sensitivity of our results to these variables we performed three additional simulations, in which we use anomalies calculated from hosing experiments with the OSUVic model (bottom panels in Fig. 11). The OSUVic model includes a fully coupled dynamical atmosphere at T42 resolution (Schmittner et al., 2011), whereas the other components are identical to the UVic model version 2.8 without dynamic vegetation. In response to an AMOC shutdown OSUVic simulates a large anticyclonic anomaly over the North Atlantic, a cyclonic anomaly over the North Pacific, a southward shift of the Intertropical Convergence Zone (ITCZ) particularly over the Atlantic, and a southward shift of Southern Hemisphere westerlies consistent with previous studies (Timmermann et al., 2007; Zhang and Delworth, 2005; Schmittner et al., 2007b). Note that the changes in Southern Hemisphere westerlies are generally less than 10 % of the absolute values of the control simulation and thus much smaller than those used by Lee et al., (2011).

The OSUVic wind anomalies are applied at model year 400 of the FW0.15 simulation (blue dashed line in panel A of Fig. 12). The wind changes have only a modest impact on simulated carbon cycle and isotope distributions (Fig. 12). The largest effect is due to changes in moisture advection velocities, which lead to a rapid decrease in vegetation and soil carbon around year 400. This causes a rapid CO_2 increase by a few ppm and a rapid decrease of $\delta^{13}C_{CO_2}$ by a few hundredths of a permil. It also delays the oceanic carbon loss by a few hundred years. However, the multi-millennial response and our conclusions are not impacted much by the wind changes.

4 Discussion

Taken together the changes in the sedimentary deep ocean $\delta^{13}C_{DIC}$ reconstructions from the LGM to the late HS1 are most consistent with simulations of a severe and prolonged, multi-millennial AMOC reduction. Model FW0.15 fits the reconstructions best as indicated by a high correlation coefficient ($r_{FW0.15} = 0.85$; Fig. 10; Table 2), a root-mean-squared error ($rms_{FW0.15} = 0.49$) just slightly larger than for models FW0.05 and FW0.1, and a standard deviation closest to the observations ($rstd_{FW0.15} = 1.75$). However, $\delta^{13}C_{DIC}$ changes in the North Atlantic are about twice as large in the model than in the reconstructions, which causes the standard deviation in model FW0.15 to be 75% larger than that of the observations. One reason for this discrepancy may be that AMOC changes during HS1 were smaller than those simulated here (Gherardi et al., 2009; Lund et al., in review). A second reason could be the mismatch in initial conditions. If the LGM AMOC was weaker and shallower than in the model's pre-industrial simulation as indicated by a number of reconstructions (Lynch-Stieglitz et al., 2007; Gebbie, 2014), the model would overestimate changes in volume fluxes and perhaps carbon isotopes even if a complete AMOC collapse did occur during HS1. A third reason may be biases in the foraminifera-based $\delta^{13}C_{DIC}$ reconstructions e.g. due to a dependency on carbonate ion concentrations (Spero et al. 1997) or dampened records of the actual $\delta^{13}C_{DIC}$ changes by smoothing and averaging due to bioturbation, and/or age model errors. The former would affect particularly regions with large changes in carbonate ion concentrations such as the North Atlantic in case of an AMOC collapse and the latter may affect particularly low resolution sediment cores as indicated by reduced agreement with lower resolution data from a previous study (Sarnthein et al., 1994) ($r_{FW0.15} = 0.80$; $rms_{FW0.15} = 0.60$; Fig. 10). Resolving the likelihood of these different possibilities will be an important task for future research.

Due to these issues our results can only be regarded as semi-quantitative. They support qualitatively McManus et al.'s (2004) interpretation of the $^{231}Pa/^{230}Th$ record, but they cannot rule out the possibility of a reduced, but not necessarily collapsed HS1 AMOC based on analyses of Atlantic carbon and oxygen isotope data (Lund et al. in review; Oppo and Curry,

in review). More work is needed for a truly quantitative reconstruction of early deglacial AMOC changes.

Our simulations suggest that an AMOC decline during HS1 could have caused the observed rise in atmospheric CO_2 and the decrease in $\delta^{13}C_{CO_2}$ by modulating the global efficiency of the ocean's biological pump. This is in contrast with ideas that invoke Southern Ocean (Toggweiler et al. 2006; Anderson et al., 2009; Tschumi et al., 2011; Lee et al., 2011) and/or North Pacific (Menviel et al., 2014) mechanisms for the early deglacial CO_2 rise. However, as discussed above, one possible explanation for the overestimated North Atlantic $\delta^{13}C_{DIC}$ changes in the model is that the early deglacial AMOC changes were smaller. If this was the case the model could possibly also overestimate the effects on atmospheric CO_2 and $\delta^{13}C_{CO_2}$ and the agreement with the ice core observations could be fortuitous.

A critical test of our hypothesis that the AMOC reduction caused a decrease of the efficiency of the biological pump may come from additional $\delta^{13}C_{DIC}$ reconstructions from the deep Pacific and Indian oceans, which hold most of the ocean's carbon and where the model predicts $\delta^{13}C_{DIC}$ to increase, but where few sedimentary data are currently available (Figs. 4, 7). Indeed, our mechanism relies on changes in the inflow of (low preformed nutrient) Atlantic deep water into the Southern, Indian, and Pacific oceans. Currently it is not known if this inflow was weaker during the LGM. Gebbie (2014) suggests a similar AMOC to the modern. Kwon et al. (2012) suggest an even stronger influence of North Atlantic water in the global deep ocean at the LGM. These findings may indicate that our simulations with modern initial conditions may also be applicable to the early deglacial, but a solid quantitative assessment remains to be performed. Such an assessment requires simulations with more realistic initial conditions, which will be an important task for future work.

Our wind stress experiments show much smaller impacts on the carbon cycle than those caused by the buoyancy forcing and suggest only a minor effect on the overall rise of atmospheric CO_2 during HS1 but they are subject to the same caveats as discussed above with respect to initial conditions. However, changes in tropical winds associated with ITCZ shits impact the hydrological cycle and terrestrial carbon and cause a jump of CO_2 by a few ppm (Fig. 12). Although this is much smaller than the 12 ppm jump recently observed around

16,250 years BP by Marcott et al. (2014) it suggests a mechanism that could explain rapid increases in atmospheric CO_2.

We have not discussed the later parts of the deglacial such as the Bølling-Allerød (15-13 ka BP), during which the AMOC was presumably reinvigorated (McManus et al. 2004). In our model this would lead to a decrease in atmospheric CO_2, whereas ice core data show stable concentrations (Monin et al., 2011; Parrenin et al., 2013; Marcott et al. 2014), suggesting an additional process counteracted the AMOC effect. We speculate that this process may be related to a deepening of the AMOC beyond LGM depths and the erosion of the deep South Atlantic reservoir of respired carbon, consistent with recent reconstructions that show that $\delta^{13}C_{DIC}$ decreases there later in the deglaciation (Lund et al., in review).

5 Conclusions

Comparison of distributed deep ocean $\delta^{13}C_{DIC}$ reconstructions with our model simulations suggests that during HS1 the AMOC was substantially reduced for several thousand years. However, due to remaining model-sediment data differences and a mismatch in initial conditions we cannot assess the likelihood of a partial AMOC reduction versus a complete shutdown.

Agreement of simulated atmospheric CO_2 and $\delta^{13}C_{CO_2}$ with ice core data, if not fortuitous, supports our hypothesis of an AMOC induced reduction of the oceans biological pump during HS1. However, this idea needs further testing with more realistic simulations in the future, improving initial conditions and transient forcing.

AMOC induced wind changes simulated in a coupled ocean-atmosphere model have only a small impact on the carbon cycle and isotope distributions in our carbon cycle model suggesting that wind changes were less important than previously thought in controlling atmospheric CO_2 and $\delta^{13}C_{CO_2}$ during HS1. However, effects of wind shifts on the hydrological cycle and terrestrial carbon could explain some of the recently observed rapid CO_2 increases (Marcott et al. 2014).

Appendix A: Model description

The University of Victoria Earth System Climate Model (UVic ESCM) (Weaver et al., 2001), is used in version 2.9 (Eby et al., 2009). It consists of a coarse resolution ($1.8^\circ \times 3.6^\circ$, 19 vertical layers) ocean general circulation model coupled to a one layer atmospheric energy-moisture balance model and a dynamic thermodynamic sea ice model, both at the same horizontal resolution. The model is forced with seasonally varying solar irradiance at the top-of-the-atmosphere, cloud albedo, wind stress, wind speed, and moisture advection velocities. This seasonal forcing does not change between different years. Atmospheric CO_2 and $\delta^{13}C$ are calculated in a single box assuming rapid mixing.

A1 Description of land carbon isotopes (δ^{13}C and δ^{14}C) model

The land carbon isotopes model has not been published before. Therefore we provide a description and evaluation here. It is based on TRIFFID, the "Top-down Representation of Interactive Foilage and Flora Including Dymamics" dynamic vegetation model by Cox (2001), as modified by Meissner et al. (2003) and Matthews et al. (2004), which solves prognostic equations for total vegetation carbon density $\mathsf{C_v} = {}^{12}\mathsf{C_v} + {}^{13}\mathsf{C_v}$ and fractional coverage $v_i \in (0,1)$ of five plant functional types (PFTs; $i = 1,\ldots,5$):

$$\frac{\partial}{\partial t}\left(\mathsf{C}_{\mathsf{v},i}\nu_i\right) = \nu_i\Pi_i - \nu_i\Lambda_i, \tag{A1}$$

where Π_i is Net Primary Production (NPP) and Λ_i is litter production, which enters the soil carbon pool. Total soil carbon density is calculated according to

$$\frac{\partial}{\partial t}\mathsf{C_s} = \sum_i \Lambda_i - R_{\mathsf{s}}. \tag{A2}$$

We added prognostic equations for the heavy carbon isotopes ^{13}C and ^{14}C to both vegetation

$$\frac{\partial}{\partial t}\left({}^{13}\mathsf{C}_{\mathsf{v},i}\nu_i\right) = \gamma^{13}_{\Pi,i}\nu_i\Pi_i - \gamma^{13}_{\Lambda,i}\nu_i\Lambda_i, \tag{A3}$$

and soil

$$\frac{\partial}{\partial t}{}^{13}\mathsf{C}_\mathsf{s} = \sum_i \gamma^{13}_{\Lambda,i}\Lambda_i - \gamma^{13}_R R_\mathsf{s}, \tag{A4}$$

$$\frac{\partial}{\partial t}\left({}^{14}\mathsf{C}_{\mathsf{v},i}\nu_i\right) = \gamma^{14}_{\Pi,i}\nu_i\Pi_i - \gamma^{14}_{\Lambda,i}\nu_i\Lambda_i - \kappa\nu_i{}^{14}\mathsf{C}_{\mathsf{v},i}, \tag{A5}$$

and

$$\frac{\partial}{\partial t}{}^{14}\mathsf{C}_\mathsf{s} = \sum_i \lambda_{\Lambda,i}\Lambda_i - \gamma^{14}_R R_\mathsf{s} - \kappa{}^{14}\mathsf{C}_{\mathsf{s,\,i}}, \tag{A6}$$

where fractionation during photosynthesis is indicated by factors

$$\gamma^{13}_\Pi = \frac{\beta^{13}_\Pi}{1+\beta^{13}_\Pi}, \tag{A7}$$

and

$$\beta^{13}_\Pi = \alpha^{13}_\Pi R^{13}_\mathsf{A}, \tag{A8}$$

where

$$R^{13}_\mathsf{A} = \frac{{}^{13}\mathsf{C}_{\mathsf{CO}_2}}{{}^{12}\mathsf{C}_{\mathsf{CO}_2}} \tag{A9}$$

is the heavy to light isotope ratio of atmospheric CO_2.

Fractionation factors are different for C_3 and C_4 plants

$$\alpha^{13}_{\mathsf{NPP},i} = \begin{Bmatrix} 0.979,\ \text{for } \mathsf{C}_3 \\ 0.993,\ \text{for } \mathsf{C}_4 \end{Bmatrix}, \tag{A10}$$

which corresponds to a fractionation of $\varepsilon^{13} = (1-\alpha^{13}) = -7‰$ for C_4 plants and $\varepsilon^{13} = -21‰$ for C_3 plants (O'Leary, 1988).

No fractionation occurs during litter production or respiration:

$$\gamma_{\Lambda}^{13} = \frac{\beta_{\Lambda}^{13}}{1+\beta_{\Lambda}^{13}} \tag{A11}$$

$$\beta_{\Lambda}^{13} = R_{\mathrm{v},i}^{13} = \frac{^{13}\mathrm{C_v}}{\mathrm{C_v} - ^{13}\mathrm{C_v}} \tag{A12}$$

$$\gamma_{R}^{13} = \frac{\beta_{R}^{13}}{1+\beta_{R}^{13}} \tag{A13}$$

$$\beta_{R}^{13} = R_{\mathrm{s}}^{13} = \frac{^{13}\mathrm{C_s}}{\mathrm{C_s} - ^{13}\mathrm{C_s}}. \tag{A14}$$

For radiocarbon Eqs. (A5) and (A6) radioactive decay is considered though $\kappa = 1.210 \times 10^{-4} a^{-1}$, which corresponds to a half life of 5730 years and twice the fractionation during NPP is assumed $\varepsilon^{14} = 2\varepsilon^{13}$, such that

$$\alpha_{\mathrm{NPP},i}^{14} = \begin{Bmatrix} 0.958, \text{for } \mathrm{C_3} \\ 0.986, \text{for } \mathrm{C_4} \end{Bmatrix}. \tag{A15}$$

The simulated spatial distribution of average δ^{13}C (Fig. 12) varies from -13 ‰ in regions dominated by C_4 grasses such as North Africa and Australia to -27 ‰ in most other regions, which are dominated by C_3 plants, due to the differences in fractionation factors for C_3 and C_4 plants used in the model. This distribution is broadly consistent with previous independent estimates (Still and Powell, 2010; Powell et al., 2012).

A2 Description of ocean carbon isotope model

We use the Model of Ocean Biogeochemistry and Isotopes (MOBI) version 1.4. The ocean carbon isotope component is described in detail in Schmittner et al. (2013). Here we only describe differences with respect to that publication. The physical UVic model version was updated to version 2.9 (Schmittner et al., 2013 used 2.8). The ocean ecosystem model

has been modified by changing zooplankton grazing, using a slightly different approach to consider iron limitation of phytoplankton growth as described in detail in (Keller et al., 2012). This model gives very similar results to model FeL, which uses a simple mask to consider iron limitation of phytoplankton growth, in Schmittner et al. (2013).

Implementation of the carbon isotope equations have been changed from the "alpha" formulation to the "beta" formulation, courtesy of Chris Somes. In the "alpha" formulation the change in the heavy (rare) isotope carbon density ^{13}C (in $\mathrm{mol\,C\,m^{-3}}$) of the product (e.g. phytoplankton) of some process (e.g. photosynthesis)

$$\frac{\partial}{\partial t}{}^{13}\mathrm{C} = \alpha R^{13}\frac{\partial}{\partial t}{}^{12}\mathrm{C} = \alpha R^{13}\frac{\partial}{\partial t}C, \tag{A16}$$

is calculated as the product of the total carbon change $\partial C/\partial t$ times the fractionation factor α for that process times the heavy to light isotope ratio of the source (e.g. sea water DIC) $R^{13} = {}^{13}C/{}^{12}\mathrm{C}$. This formulation assumes total carbon

$$C = {}^{12}\mathrm{C} + {}^{13}\mathrm{C} \approx {}^{12}\mathrm{C}, \tag{A17}$$

is equal to ^{12}C, which is a good approximation since ^{13}C is usually two orders of magnitude smaller than ^{12}C.

However, assumption (A17) can be avoided by using the "beta" formulation, in which the heavy isotope change is calculated according to

$$\frac{\partial}{\partial t}{}^{13}\mathrm{C} = \frac{\beta^{13}}{1+\beta^{13}}\frac{\partial}{\partial t}\mathrm{C}, \tag{A18}$$

where $\beta^{13} = \alpha^{13}R^{13}$.

In order to convert isotope ratios to delta values

$$\delta^{13}\mathrm{C} = (R/R_{\mathrm{std}} - 1) \tag{A19}$$

we now use the conventional standard ratio $R^{13}_{\mathrm{std}} = 0.0112372$ instead of $R^{13}_{\mathrm{std}} = 1$, which was used in (Schmittner et al., 2013). For radiocarbon $R^{14}_{\mathrm{std}} = 1.17 \times 10^{-12}$ is used.

MOBI 1.4 includes dissolved organic carbon (DOC) cycling described in Somes et al. (2014). The close agreement of the preindustrial $\delta^{13}C_{DIC}$ distributions with model FeL of Schmittner et al. (2013) suggest that none of the changes described above have a major impact of the simulated $\delta^{13}C_{DIC}$.

Acknowledgements. AS has been supported by the National Science Foundation's Marine Geology and Geophysics program grant OCE-1131834. Most reconstructions listed in Table 2 were extracted from the National Oceanic and Atmospheric Administration's (NOAA) National Climatic Data Center (NCDC) Paleoclimatology Program Database (http://www.ncdc.noaa.gov/data-access/paleoclimatology-data). We are grateful to all data generators who make their data available on public databases. We are also thankful to Claire Waelbroeck, Rainer Zahn, and Ros Rickaby for generously sharing data used in this study. Thanks to Christopher Somes for re-writing the carbon isotope model in the "beta" formulation.

References

Anderson, R. and Hayes, C.: New insights into gochemical proxies from GEOTRACES, 11th International Conference on Paleoceanography, Sitges, Spain, 2013.

Anderson, R. F., Ali, S., Bradtmiller, L. I., Nielsen, S. H. H., Fleisher, M. Q., Anderson, B. E., and Burckle, L. H.: Wind-driven upwelling in the Southern Ocean and the deglacial rise in atmospheric CO_2, Science, 323, 1443–1448, doi:10.1126/Science.1167441, 2009.

Bard, E., Rostek, F., Turon, J-L., and Gendreau, S.: Hydrological impact of Heinrich Events in the subtropical northeast Atlantic, Science, 289, 1321–1324, 2010.

Benway, H. M., McManus, J. F., Oppo, D. W., and Cullen, J. L.: Hydrographic changes in the eastern sub polar North Atlantic during the last deglaciation, Quaternary Sci. Rev., 29, 3336–3345, doi:10.1016/j.quascirev.2010.08.013, 2010.

Blunier, T., Chappellaz, J., Schwander, J., Dällenbach, A., Staffer, B., Stocker, T. F., Raynaud, D., Jouzel, J., Clausen, H. B., Hammer, C. U., and Johnsen, S. J.: Asynchrony of Antarctic and Greenland climate change during the last glacial period, Nature, 394, 739–743, 1998.

Bozbiyik, A., Steinacher, M., Joos, F., Stocker, T. F., and Menviel, L.: Fingerprints of changes in the terrestrial carbon cycle in response to large reorganizations in ocean circulation, Clim. Past, 7, 319–338, doi:10.5194/cp-7-319-2011, 2011.

Boyle, E. A., and Keigwin, L. D.: Deep circulation of the North Atlantic over the last 200,000 years: Geochemical evidence, Science, 218, 784–787, 1982.

Broecker, W. S., Peteet, D. M., and Rind, D.: Does the ocean–atmosphere system have more than one stable mode of operation?, Nature, 315, 21–26, 1985.

Charles, C. D., Lynch-Stieglitz, J., Ninnemann, U. S., and Fairbanks, R. G.: Climate connections between the hemisphere revealed by deep sea sediment core ice core correlations, Earth Planet. Sc. Lett., 142, 19–27, 1996.

Clark, P. U., McCabe, A. M., Mix, A. C., and Weaver, A. J.: Rapid rise of sea level 19 000 years ago and its global implications, Science, 304, 1141–1144, doi:10.1126/Science.1094449, 2004.

Cox, P.: Description of the "TRIFFID" Dynamic Global Vegetation Model, Hadley Center, Technical Note 24, 1–16, 2001.

Crowley, T. J.: North Atlantic Deep Water cools the southern hemisphere, Paleoceanography, 7, 489-497, 1992.

Curry, W. B. and Oppo, D. W.: Glacial water mass geometry and the distribution of delta C-13 of Sigma CO_2 in the western Atlantic Ocean, Paleoceanography, 20, PA1017, doi:10.1029/2004PA001021, 2005.

Denton, G., Broecker, W. S., and Alley, R. B.: The mystery invervall 17.5 to 14.5 kyr ago, PAGES News, 14, 14–16, 2006.

Denton, G. H., Anderson, R. F., Toggweiler, J. R., Edwards, R. L., Schaefer, J. M., and Putnam, A. E.: The last glacial termination, Science, 328, 1652–1656, doi:10.1126/science.1184119, 2010.

Eby, M., Zickfeld, K., Montenegro, A., Archer, D., Meissner, K. J., and Weaver, A. J.: Lifetime of anthropogenic climate change: millennial time scales of potential CO_2 and surface temperature perturbations, J. Climate, 22, 2501–2511, doi:10.1175/2008jcli2554.1, 2009.

Gebbie, G.: How much did glacial North Atlantic water shoal?, Paleoceanography, 29, 190–209, doi:10.1002/2013PA002557, 2014.

EPICA community members: One-to-one coupling of glacial climate variability in Greenland and Antarctica, Nature, 444, 195–198, doi:10.1038/nature05301, 2006.

Gherardi, J., Labeyrie, L., Nave, S., Francois, R., McManus, J., and Cortijo, E.: Glacial-interglacial circulation changes inferred from $^{231}Pa/^{230}Th$, Paleoceanogr., 24, PA2204, doi:10.1029/2008PA001696, 2009.

He, F., Shakun, J. D., Clark, P. U., Carlson, A. E., Liu, Z., Otto-Bliesner, B. L., and Kutzbach, J. E.: Northern Hemisphere forcing of Southern Hemisphere climate during the last deglaciation, Nature, 494, 81–85, doi:10.1038/nature11822, 2013.

Hodell, D. A., Evans, H. F., Channell, J. E. T., and Curtis, J. H.: Phase relationships of North Atlantic ice-rafted debris and surface-deep climate proxies during the last glacial period, Quaternary Sci. Rev., 29, 3875–3886, doi:10.1016/J.Quascirev.2010.09.006, 2010.

Hoffman, J., and Lund, D. C.: Refining the stable isotope budget for Antarctic Bottom Water: New results from the abyssal southwestern Atlantic, Paleoceanogr., 27, PA1213, doi:10.1029/2011PA002216, 2012.

Ito, T. and Follows, M. J.: Preformed phosphate, soft tissue pump and atmospheric CO_2, J. Mar. Res., 63, 813–839, 2005.

Jung, S. J. A., Kroon, D., Ganssen, G., Peeters, F., and Ganeshram, R.: Enhanced Arabian Sea intermediate water flow during glacial North Atlantic cold phases, Earth Planet. Sc. Lett., 280, 220–228, 2009.

Kalnay, E., Kanamitsu, M., Kistler, R., Collins, W., Deaven, D., Gandin, L., Iredell, M., Saha, S., White, G., Woollen, J., Zhu, Y., Chelliah, M., Ebisuzaki, W., Higgins, W., Janowiak, J., Mo, K. C., Ropelewski, C., Wang, J., Leetmaa, A., Reynolds, R., Jenne, R., and Joseph, D.: The NCEP/NCAR 40 year reanalysis project, B. Am. Meteorol. Soc., 77, 437–471, 1996.

Keigwin, L. D. and Boyle, E. A.: Did North Atlantic overturning halt 17,000 years ago?, Paleoceanography, 23, PA1101, doi:10.1029/2007PA001500, 2008.

Keller, D. P., Oschlies, A., and Eby, M.: A new marine ecosystem model for the University of Victoria Earth System Climate Model, Geosci. Model Dev., 5, 1195–1220, doi:10.5194/gmd-5-1195-2012, 2012.

Köhler, P., Joos, F., Gerber, S., and Knutti, R.: Simulated changes in vegetation distribution, land carbon storage, and atmospheric CO_2 in response to a collapse of the North Atlantic thermohaline circulation, Clim. Dyn., 25, 689–708, doi:10.1007/s00382-005-0058-8, 2005.

Kurahashi-Nakamura, T., Losch, M., and Paul, A.: Can sparse proxy data constrain the strength of the Atlantic meridional overturning circulation?, Geosci. Model Dev., 7, 419–432, doi:10.5194/gmd-7-419-2014, 2014.

Kwon, E. Y., Hein, M. P., Sigman, D. M., Galbraith, E. D., Sarmiento, J. L., and Toggweiler, J. .R.: North Atlantic ventilation of "southern-sourced" deep water, Paleoceanography, 27, PA2208, doi:10.1029/2011PA002211, 2012.

Labeyrie, L., Waelbroeck, C., Cortijo, E., Michel, E., and Duplessy, J. C.: Changes in deep water hydrology during the Last Deglaciation, CR Geosci., 337, 919–927, doi:10.1016/J.Crte.2005.05.010, 2005.

Lourantou, A., Lavric, J. V., Kohler, P., Barnola, J. M., Paillard, D., Michel, E., Raynaud, D., and Chappellaz, J.: Constraint of the CO2 rise by new atmospheric carbon isotopic measurements during the last deglaciation, Global Biogeochem Cy, 24, GB2015, doi:10.1029/2009gb003545, 2010.

Lund, D. C., Tessin, A. C., Hoffman, J. L., and Schmittner, A.: Southwest Atlantic watermass evolution during the last deglaciation, Paleoceanography, in review.

Lund, D. C., Mix, A. C., and Southon, J.: Increased ventilation age of the deep northeast Pacific Ocean during the last deglaciation, Nature Geoscience, 4, 771–774, doi:10.1038/NGEO1272, 2011.

Lynch-Stieglitz, J., Adkins, J. F., Curry, W. B., Dokken, T., Hall, I. R., Herguera, J. C., Hirschi, J. J. M., Ivanova, E. V., Kissel, C., Marchal, O., Marchitto, T. M., McCave, I. N., McManus, J. F., Mulitza, S., Ninnemann, U., Peeters, F., Yu, E. F., and Zahn, R.: Atlantic meridional overturning circulation during the Last Glacial Maximum, Science, 316, 66–69, doi:10.1126/Science.1137127, 2007.

Lynch-Stieglitz, J., Schmidt, M. W., Henry, L. G. Curry, W. B., Skinner, L. C., Mulitza, S., Zhang, R., and Chang, P.: Muted change in Atlantic overturning circulation over some glacial-aged Heinrich events, Nature Geosc., 7, 144–150, doi:10.1038/NGEO2045, 2014.

Marchal, O., Stocker, T. F., and Joos, F.: Impact of oceanic reorganizations on the ocean carbon cycle and atmospheric carbon dioxide content, Paleoceanography, 13, 225–244, 1998.

Marchal, O., Stocker, T. F., Joos, F., Indermühle, A., Blunier, T., and Tschumi, J.: Modeling the concentration of atmospheric CO_2 during the Younger Dryas climate event, Climate Dynamics, 15, 341–354, 1999.

Marinov, I., Follows, M., Gnanadesikan, A., Sarmiento, J. L., and Slater, R. D.: How does ocean biology affect atmospheric $p\mathrm{CO}_2$? Theory and models, J. Geophys. Res., 113, C07032, doi:10.1029/2007jc004598, 2008a.

Marinov, I., Gnanadesikan, A., Sarmiento, J. L., Toggweiler, J. R., Follows, M., and Mignone, B. K.: Impact of oceanic circulation on biological carbon storage in the ocean and atmospheric $p\mathrm{CO}_2$, Global Biogeochem. Cy., 22, GB3007, doi:10.1029/2007GB002958, 2008b.

Matthews, H. D., Weaver, A. J., Meissner, K. J., Gillett, N. P., and Eby, M.: Natural and anthropogenic climate change: incorporating historical land cover change, vegetation dynamics and the global carbon cycle, Clim. Dynam., 22, 461–479, doi:10.1007/s00382-004-0392-2, 2004.

McManus, J. F., Francois, R., Gherardi, J. M., Keigwin, L. D., and Brown-Leger, S.: Collapse and rapid resumption of Atlantic meridional circulation linked to deglacial climate changes, Nature, 428, 834–837, 2004.

Meissner, K. J., Weaver, A. J., Matthews, H. D., and Cox, P. M.: The role of land surface dynamics in glacial inception: a study with the UVic Earth System Model, Clim. Dynam., 21, 515–537, doi:10.1007/S00382-003-0352-2, 2003.

Menviel, L., Timmermann, A., Mouchet, A., and Timm, O.: Meridional reorganizations of marine and terrestrial productivity during Heinrich events, Paleoceanography, 23, PA1203, doi:10.1029/2007pa001445, 2008.

Menviel, L., Joos, F., and Ritz, S. P.: Simulating atmospheric CO_2, ^{13}C and the marine carbon cycle during the Last GlacialeInterglacial cycle: possible role for a deepening of the mean remineralization depth and an increase in the oceanic nutrient inventory, Quat. Sci. Rev., 56, 46–68, doi:10.1016/j.quascirev.2012.09.012, 2012.

Menviel, L., England, M. H., Meissner, K. J., Mouchet, A., and Yu, J.: Atlantic-Pacific seesaw and its role in outgassing CO2 during Heinrich events, Paleoceanography, 29, 58–70, doi:10.1002/2013pa002542, 2014.

Mix, A. C., Lund, D. C., Pisias, N. G., Boden, P., Bornmalm, L., Lyle, M., and Pike, J.: Rapid climate oscillations in the Northeast Pacific during the last deglaciation reflect northern and southern sources, in Mechanisms of Global Climate Change at Millennial Time Scales, edited by Clark, P., R. S. Webb, and L. D. Keigwin, Geophysical Monograph Series, 112, American Geophysical Union, Washington DC, pp. 127–148, 1999.

Monnin, E., Indermühle, A., Dällenbach, A., Flückiger, J., Stauffer, B., Stocker, T. F., Raynaud, D., and Barnola, J.-M.: Atmospheric CO_2 concentrations over the Last Glacial Termination, Science, 291, 112–114, doi:10.1126/science.291.5501.112, 2001.

Obata, A.: Climate-carbon cycle model response to Freshwater discharge into the North Atlantic, J. Climate, 20, 5962–5976, 2007.

O'Leary, M. H.: Carbon isotopes in photosynthesis, Bioscience, 38, 328–336, 1988.

Oppo, D. W., and Curry, W. B.: What can benthic $\delta^{13}C$ and $\delta^{18}O$ data tell us about the Atlantic circulation during Heinrich Stadial 1?, Paleoceanogr., in review.

Pahnke, K. and Zahn, R.: Southern Hemisphere water mass conversion linked with North Atlantic climate variability, Science, 307, 1741–1746, 2005.

Parrenin, F., Masson-Delmotte, V., Köhler, P., Raynaud, D., Paillard, D., Schwander, J., Barbante, C., Landais, A., Wegner, A., and Jouzel, J.: Synchronous change of atmospheric CO_2 and Antarctic temperature during the last deglacial warming, Science, 339, 1060–1063, doi:10.1126/science.1226368, 2013.

Peck, V. L., Hall, I. R., Zahn, R., and Scourse, J. D.: Progressive reduction in NE Atlantic intermediate water ventilation prior to Heinrich events: Response to NW European ice sheet instabilities?, Geochem. Geophys. Geosyst., 8, Q01N10, doi:10.1029/2006GC001321, 2005.

Petit, J. R., Jouzel, J., Raynaud, D., Barkov, N. I., Barnola, J. M., Basile, I., Bender, M., Chappellaz, J., Davis, M., Delaygue, G., Delmotte, M., Kotlyakov, V. M., Legrand, M., Lipenkov, V. Y., Lorius, C., Pepin, L., Ritz, C., Saltzman, E., and Stievenard, M.: Climate and atmospheric history of the past 420 000 years from the Vostok ice core, Antarctica, Nature, 399, 429–436, 1999.

Powell, R. L., Yoo, E.-H., and Still, C. J.: Vegetation and soil carbon-13 isoscapes for South America: integrating remote sensing and ecosystem isotope measurements, Ecosphere, 3, art109, doi:10.1890/ES12-00162.1, 2012.

Praetorius, S. K., McManus, J. F., Oppo, D. W., and Curry, W. B.: Episodic reductions in bottom-water currents since the last ice age, Nat Geosci, 1, 449–452, doi:10.1038/ngeo227, 2008.

Rickaby, R. E. M. and Elderfield, H.: Evidence from the high-latitude North Atlantic for variations in Antarctic intermediate water flow during the last deglaciation, Geochem. Geophy. Geosy., 6, Q05001, doi:10.1029/2004GC000858, 2005.

Saenko, O., Schmittner, A., and Weaver, A. J.: The Atlantic–Pacific Seesaw, J. Climate, 17, 2033–2038, 2004.

Sarnthein, M., Winn, K., Jung, S. J., Duplessy, J. C., Labeyrie, L., Erlenkeuser, H., and Ganssen, G.: Changes in east Atlantic deepwater circulation over the last 30 000 years: eight time slice reconstructions, Paleoceanography, 9, 209–267, 1994.

Schmitt, J., Schneider, R., Elsig, J., Leuenberger, D., Lourantou, A., Chappellaz, J., Köhler, P., Joos, F., Stocker, T. F., Leuenberger, M., and Fischer, H.: Carbon isotope constraints on the deglacial CO_2 rise from ice cores, Science, 336, 711–714, doi:10.1126/science.1217161, 2012.

Schmittner, A., Saenko, O. A., and Weaver, A. J.: Coupling of the hemispheres in observations and simulations of glacial climate change, Quaternary Sci. Rev., 22, 659–671, 2003.

Schmittner, A.: Decline of the marine ecosystem caused by a reduction in the Atlantic overturning circulation, Nature, 434, 628–633, 2005.

Schmittner, A. and Galbraith, E. D.: Glacial greenhouse-gas fluctuations controlled by ocean circulation changes, Nature, 456, 373–376, doi:10.1038/nature07531, 2008.

Schmittner, A., Brook, E. J., and Ahn, J.: Impact of the ocean's overturning circulation on atmospheric CO_2, in: Ocean Circulation: Mechanisms and Impacts, edited by: Schmittner, A., Chiang, J. C. H., and Hemming, S. R., Geophysical Monograph Series, 173, American Geophysical Union, Washington DC, 315–334, 2007a.

Schmittner, A., Galbraith, E. D., Hostetler, S. W., Pedersen, T. F., and Zhang, R.: Large fluctuations of dissolved oxygen in the Indian and Pacific oceans during Dansgaard-Oeschger oscillations caused by variations of North Atlantic Deep Water subduction, Paleoceanography, 22, PA3207, doi:10.1029/2006PA001384, 2007b.

Schmittner, A., Silva, T. A., Fraedrich, K., Kirk, E., and Lunkeit, F.: Effects of mountains and ice sheets on global ocean circulation, J. Climate, 24, 2814–2829, doi:10.1175/2010JCLI3982.1, 2011.

Schmittner, A., Gruber, N., Mix, A. C., Key, R. M., Tagliabue, A., and Westberry, T. K.: Biology and air–sea gas exchange controls on the distribution of carbon isotope ratios (δ^{13}C) in the ocean, Biogeosciences, 10, 5793–5816, doi:10.5194/bg-10-5793-2013, 2013.

Scholze, M., Knorr, W., and Heimann, M.: Modelling terrestrial vegetation dynamics and carbon cycling for an abrupt climatic change event, The Holocene, 13, 327–333, 2003.

Shakun, J. D., Clark, P. U., He, F., Marcott, S. A., Mix, A. C., Liu, Z. Y., Otto-Bliesner, B., Schmittner, A., and Bard, E.: Global warming preceded by increasing carbon dioxide concentrations during the last deglaciation, Nature, 484, 49–54, doi:10.1038/Nature10915, 2012.

Sigman, D. M., de Boer, A. M., and Haug, G. H.: Antarctic stratification, atmospheric water vapor, and Heinrich Events: A hypothesis for late Pleistocene Deglaciations, in: Ocean Circulation: Mechanisms and Impacts, edited by: Schmittner, A., Chiang, J. C. H., and Hemming, S. R., Geophysical Monograph Series, 173, American Geophysical Union, Washington DC, 315–334, 2007a.

Sirocko, F., Sarnthein, M., Erlenkeuser, H., Lange, H., Arnold, M., and Duplessy, J. C.: Century-scale events in monsoonal climate over the past 24,000 years, Nature, 364, 322–324, 1993.

Skinner, L. C. and Shackleton, N.: Rapid transient changes in Northeast Atlantic deep water ventilation age across termination I, Paleoceanography, 19, doi:10.1029/2003pa000983, 2004.

Sortor, R. N. and Lund, D. C.: No evidence for a deglacial intermediate water Δ^{14}C anomaly in the SW Atlantic, Earth and Planetary Science Letter, 310, 65–72, doi:doi:10.1016/j.epsl.2011.07.017, 2011.

Spero, H. J. and Lea, D. W.: The cause of carbon isotope minimum events on glacial terminations, Science, 296, 522–525, doi:10.1126/Science.1069401, 2002.

Stern, J. V. and Lisiecki, L. E.: North Atlantic circulation and reservoir age changes over the past 41,000 years, Geophys. Res. Lett., 40, 3693–3697, doi:10.1002/grl.50679, 2013.

Still, C. J. and Powell, R. L.: Continental-Scale Distributions of Vegetation Stable Carbon Isotope Ratios, in, edited by: West, J. B., Bowen, G. J., Dawson, T. E., and Tu, K. P., Springer Netherlands, Dordrecht, 179–193, 2010.

Stommel, H.: Thermohaline convection with two stable regimes of flow, Tellus, 13, 224–230, 1961.

Stott, L., Timmermann, A., and Thunell, R.: Southern Hemisphere and deep-sea warming led deglacial atmospheric CO_2 rise and tropical warming, Science, 318, 435–438, doi:10.1126/Science.1143791, 2007.

Tessin, A. C. and Lund, D. C.: Isotopically depleted carbon in the mid-depth South Atlantic during the last deglaciation, Paleoceanography, 28, 296–306, doi:10.1002/palo.20026, 2013.

Thornalley, D. J. R., Elderfield, H., and McCave, I. N.: Intermediate and deep water paleoceanography of the northern North Atlantic over the past 21,000 years, Paleoceanography, 25, PA1211, doi:10.1029/2009pa001833, 2010.

Timmermann, A., Okumura, Y., An, S. I., Clement, A., Dong, B., Guilyardi, E., Hu, A., Jungclaus, J. H., Renold, M., Stocker, T. F., Stouffer, R. J., Sutton, R., Xie, S. P., and Yin, J.: The influence of a weakening of the Atlantic meridional overturning circulation on ENSO, J. Climate, 20, 4899–4919, doi:10.1175/Jcli4283.1, 2007.

Timmermann, A., Timm, O., Stott, L., and Menviel, L.: The roles of CO_2 and orbital forcing in driving Southern Hemispheric temperature variations during the Last 21 000 yr, J. Climate, 22, 1626–1640, doi:10.1175/2008jcli2161.1, 2009.

Toggweiler, J. R., Russell, J. L., and Carson, S. R.: Midlatitude westerlies, atmospheric CO_2, and climate change during the ice ages, Paleoceanography, 21, Pa2005, doi:10.1029/2005pa001154, 2006.

Tschumi, T., Joos, F., Gehlen, M., and Heinze, C.: Deep ocean ventilation, carbon isotopes, marine sedimentation and the deglacial CO_2 rise, Clim. Past, 7, 771–800, doi:10.5194/cp-7-771-2011, 2011.

Vidal, L., Labeyrie, L., Cortijo, E., Arnold, M., Duplessy, J. C., Michel, E., Becque, S., and vanWeering, T. C. E.: Evidence for changes in the North Atlantic Deep Water linked to meltwater surges during the Heinrich events, Earth Planet. Sc. Lett., 146, 13–27, doi:10.1016/S0012-821x(96)00192-6, 1997.

Völker, L., and Köhler, P.: Responses of ocean circulation and carbon cycle to changes in the position of the Southern Hemisphere westerlies during the Last Glacial Maximum, Palaeoceaogr., 28, 726–739, doi:10.1002/2013PA002556, 2013.

Watson, A. J., and Naveira Garabato, A.: The role of Southern Ocean mixing and upwelling in glacial-interglacial atmospheric CO_2, Tellus, 58B, 73–87, doi:10.1111/j.1600-0889.2005.00167.x, 2011.

Waelbroeck, C., Skinner, L. C., Labeyrie, L., Duplessy, J. C., Michel, E., Vazquez Riveiros, N., Gherardi, J. M., and Dewilde, F.: The timing of deglacial circulation changes in the Atlantic, Paleoceanography, 26, PA3213, doi:10.1029/2010pa002007, 2011.

Weaver, A. J., Eby, M., Wiebe, E. C., Bitz, C. M., Duffy, P. B., Ewen, T. L., Fanning, A. F., Holland, M. M., MacFadyen, A., Matthews, H. D., Meissner, K. J., Saenko, O., Schmittner, A., Wang, H. X., and Yoshimori, M.: The UVic Earth System Climate Model: model description, climatology, and applications to past, present and future climates, Atmos. Ocean, 39, 361–428, 2001.

Zahn, R. and Stuber, A.: Suborbital intermediate water variability inferred from paired benthic foraminiferal Cd/Ca and delta C-13 in the tropical West Atlantic and linking with North Atlantic climates, Earth Planet. Sc. Lett., 200, 191–205, doi:10.1016/S0012-821x(02)00613-1, 2002.

Zahn, R., Schonfeld, J., Kudrass, H. R., Park, M. H., Erlenkeuser, H., and Grootes, P.: Thermohaline instability in the North Atlantic during meltwater events: stable isotope and ice-rafted detritus records from core SO75-26KL, Portuguese margin, Paleoceanography, 12, 696–710, doi:10.1029/97pa00581, 1997.

Zhang, R. and Delworth, T. L.: Simulated tropical response to a substantial weakening of the Atlantic thermohaline circulation, J. Climate, 18, 1853–1860, doi:10.1175/Jcli3460.1, 2005.

Ziegler, M., Diz, P., Hall, I. R., and Zahn, R.: Millennial-scale changes in atmospheric CO2 levels linked to the Southern Ocean carbon isotope gradient and dust flux, Nat. Geosci., 6, 457–461, doi:10.1038/ngeo1782, 2013.

Table 1. Sediment cores used in this study. Note that cores 1 and 2 have been averaged for the comparison with the model simulations shown in Figs. 7,8,10 and Tab. 2.

	Core	Longitude	Latitude	Depth (m)	References	Age Model (if different)
1	ODP984	61° N	24° W	1,649	Praetorius et al. (2008)	Lund et al. (2014)
2	NEAP4K	61° N	24° W	1,627	Rickaby and Elderfield (2005)	
3	RAPiD-10-1P	62° N	17° W	1,237	Thornalley et al. (2010)	Lund et al. (2014)
4	ODP980	55° N	15° W	2,179	Benway et al. (2010)	
5	NA87-22	55° N	14° W	2,161	Vidal et al. (1997)	Waelbroeck et al. (2011)
6	KN166-14-JPC-13	53° N	33° W	3,082	Hodell et al. (2010)	
7	MD01-2461	52° N	13° W	1,153	Peck et al. (2007)	see text (section 2)
8	SO75-26KL	37° N	10° W	1,099	Zahn et al. (1997)	Lund et al. (2014)
9	MD99-2334K	37° N	10° W	3,146	Skinner and Shackleton (2004)	
10	MD95-2037	37° N	32° W	2,159	Labeyrie et al. (2005)	Waelbroeck et al. (2011)
11	KNR166-2-26JPC	24° N	83° W	546	Lynch-Stieglitz et al. (2014)	
12	M35003-4	12° N	61° W	1,299	Zahn and Stuber (2002)	Lund et al. (2014)
13	KNR159-5 90GGC	28° S	46° W	1,105	Lund et al. (2014); Curry and Oppo (2005)	
14	KNR159-5 36GGC	28° S	46° W	1,268	Curry and Oppo (2005); Sortor and Lund (2011)	
15	KNR159-5 17JPC	28° S	46° W	1,627	Tessin and Lund (2013)	
16	KNR159-5 78GGC	28° S	46° W	1,820	Tessin and Lund (2013)	
17	KNR159-5 33GGC	28° S	46° W	2,082	Tessin and Lund (2013)	
18	KNR159-5 42JPC	28° S	46° W	2,296	Curry and Oppo (2005); Tessin and Lund (2013)	
19	KNR159-5 30GGC	28° S	46° W	2,500	Tessin and Lund (2013)	
20	KNR159-5 125GGC	30° S	45° W	3,589	Tessin and Lund (2013); Hoffman and Lund (2012)	
21	RC11-83	41° S	9° E	4,718	Charles et al. (1996)	
22	MD01-2588	41° S	25° E	2,907	Ziegler et al. (2013)	
23	74KL	14° N	57° E	3,212	Sirocko et al. (1993)	
24	NIOP905	10° N	52° E	1,580	Jung et al. (2009)	
25	MD97-2120	45° S	174° E	1,210	Pahnke and Zahn (2005)	
26	W8709A-13PC	42° N	126° W	2,710	Lund et al. (2011); Mix et al. (1999)	

Table 2. Statistical indices of comparison for the reconstructed HS1 (15.5–16.5 ka BP) minus LGM (18.5–19.5 ka BP) ocean δ^{13}C changes with those from the model simulations (model years 2000–3000 mean minus years -1000–0 mean): correlation coefficients (r), root-mean-squared errors (rms), bias (model mean minus observed mean), and the ratio of model over observed standard deviations (rstd). The number of datapoints is $n = 25$.

Model	r	rms	bias	rstd
FW0.05	0.76	0.45	0.26	0.02
FW0.1	0.76	0.45	0.26	0.03
FW0.15	0.85	0.49	-0.29	1.75
FW0.2	0.85	0.64	-0.38	2.11

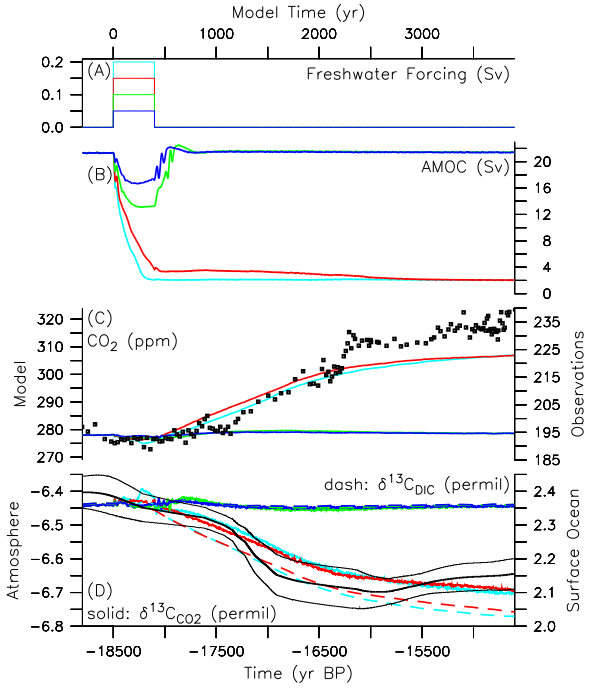

Discussion Paper | Discussion Paper | Discussion Paper | Discussion Paper |

Figure 1. Time series of **(A)** North Atlantic freshwater forcing, **(B)** AMOC response, **(C)** atmospheric CO_2 concentrations, **(D)** $\delta^{13}C$ of atmospheric CO_2 (solid, left axis) and global mean surface ocean $\delta^{13}C_{DIC}$ (dashed, right axis) for four model simulations (color lines). Symbols in **(C)** and thick black curve (error estimates are indicated by thin lines) in **(D)** show ice core measurements (Marcott et al., 2014, Schmitt et al., 2012), respectively (bottom and right (in (C)) axes).

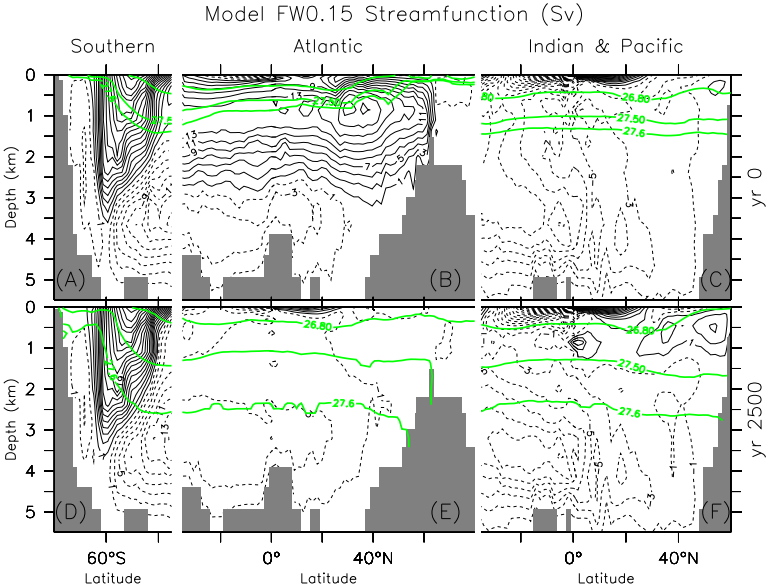
Model FW0.15 Streamfunction (Sv)
Southern
Atlantic
Indian & Pacific
Depth (km)
yr 0
yr 2500
(A)
(B)
(C)
(D)
(E)
(F)
26.80
27.50
27.6
60°S
0°
40°N
Latitude

Figure 2. Meridional overturning streamfunction (black contour lines; solid/dashed lines denote negative/positive values and clockwise/counterclockwise flow) in the Southern **(A,D)**, Atlantic **(B,E)**, and Indian and Pacific **(C,F)** oceans at year 0 (averaged from year -1,000 to 0) **(A,B,C)** and 2,500 (averaged from year 2,000 to 3,000) **(D,E,F)**. Three zonally averaged potential density (σ_Θ) isolines (27.63, 27.5, 26.8) are shown as green lines.

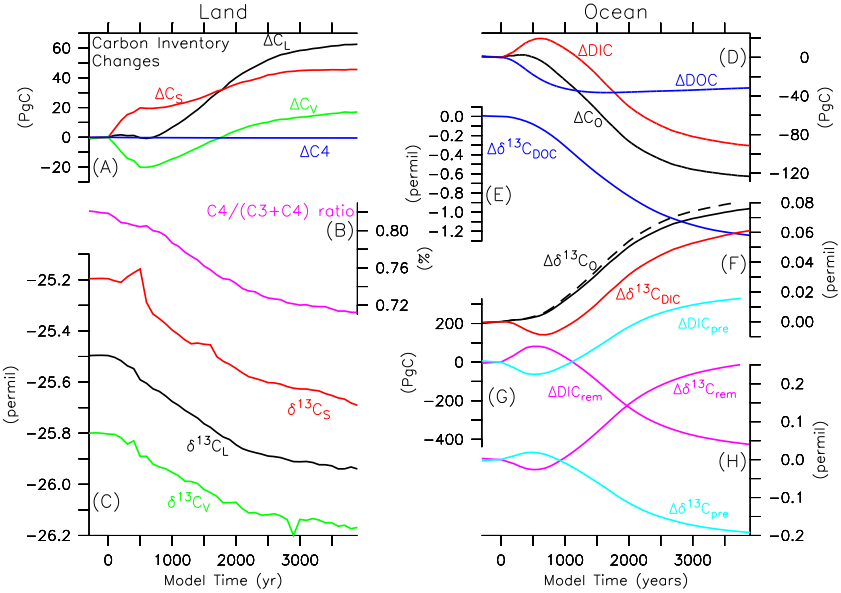
Land
Carbon Inventory Changes
ΔC_L
ΔC_S
ΔC_V
ΔC4
(PgC)
(A)
C4/(C3+C4) ratio
(B)
(C)
δ13C_S
δ13C_L
δ13C_V
(permil)
Model Time (yr)
Ocean
ΔDIC
ΔDOC
ΔC_O
(D)
(E)
Δδ13C_DOC
Δδ13C_O
Δδ13C_DIC
ΔDIC_pre
ΔDIC_rem
Δδ13C_rem
Δδ13C_pre
(F)
(G)
(H)
(%)
Model Time (years)

Figure 3. Simulated changes in global land (left) and ocean (right) carbon inventories (in Pg C; 1 ppm = 2.1 Pg C) and their averaged $\delta^{13}C$ (in permil) in model FW0.15. Changes in **(A)** land carbon $\Delta C_L = \Delta C_V + \Delta C_S$ (black) are due to vegetation ΔC_V (green) and soil ΔC_S (red) changes. Vegetation is composed of C_3 and C_4 plants, $C_V = C_3 + C_4$, but C_4 plants contribute only a small fraction **(B)** to the total. Changes in C_4 plant biomass (blue line in **A**) are negligible compared to those of C_3 plants (difference between green and blue lines). Panel **(C)** shows biomass weighted mean $\delta^{13}C$ of the land $\delta^{13}C_L = (\sum_i C_{v,i} \cdot \delta^{13}C_i + C_s \cdot \delta^{13}C_s)/(\sum_i C_{v,i} + C_s)$ (black), vegetation $\delta^{13}C_v = (\sum_i C_{v,i} \cdot \delta^{13}C_i)/(\sum_i C_{v,i})$ (green), and soil $\delta^{13}C_s$ (red). Ocean carbon changes $\Delta C_O = \Delta DIC + \Delta DOC \underbrace{+\Delta POC}_{\sim 0}$ (**D**, black) are due to dissolved organic (DOC, blue) and inorganic (DIC, red) carbon, and negligible changes in particulate organic carbon (POC, not shown). Total ocean $\delta^{13}C_O = (DIC \cdot \delta^{13}C_{DIC} + DOC \cdot \delta^{13}C_{DOC})/(DIC + DOC)$ (**F**, black) is dominated by changes in $\delta^{13}C_{DIC}$ (red). $\delta^{13}C_{DOC}$ (blue line in panel **E**) changes play only a minor role for $\Delta\delta^{13}C_O$ as illustrated by the dashed black line in **(F)**, which was calculated assuming a constant $\delta^{13}C_{DOC} = -21.5$ ‰. However, the relative contribution of DOC to C_O decreases by about 10 %, which explains the difference between the solid red and dashed black lines in **(F)**. DIC changes are further separated into remineralized (DIC_{rem}, $\Delta\delta^{13}C_{rem}$, purple) and preformed (DIC_{pre}, $\Delta\delta^{13}C_{pre}$, light blue) components in **(G)** and **(H)** following Schmittner et al. (2014). All anomalies are shown relative to model year 0, at which absolute numbers are $C_L = 1785$ Pg C, $C_O = 37\,390$ Pg C, $C_{DIC} = 37\,191$ Pg C, $C_{DOC} = 297$ Pg C, C_{POC}=2 Pg C, $\delta^{13}C_{DIC} = 0.72$ ‰, $\delta^{13}C_{DOC} = -21.5$ ‰.

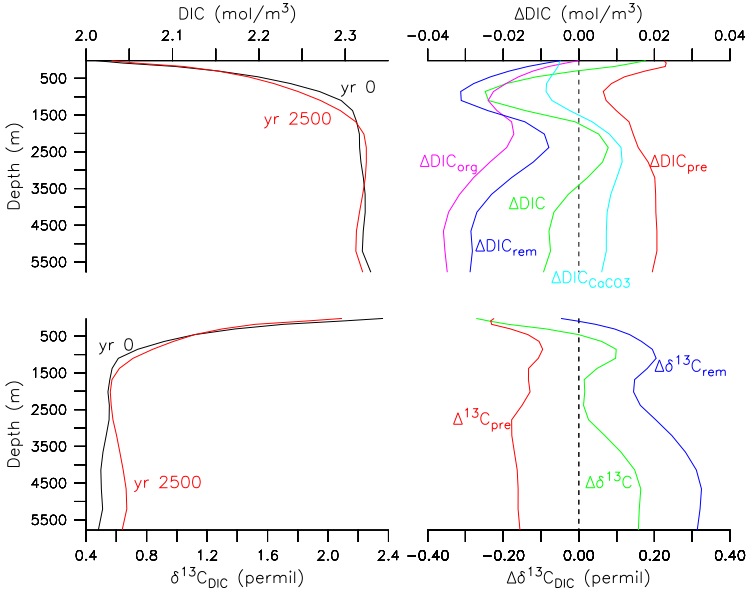
DIC (mol/m3)
2.0
2.1
2.2
2.3
yr 0
yr 2500
Depth (m)
500
1500
2500
3500
4500
5500
ΔDIC (mol/m3)
−0.04
−0.02
0.00
0.02
0.04
ΔDICorg
ΔDICpre
ΔDIC
ΔDICrem
ΔDICCaCO3
0.4
0.8
1.2
1.6
2.0
2.4
δ13CDIC (permil)
−0.40
−0.20
0.00
0.20
0.40
Δδ13CDIC (permil)
Δ13Cpre
Δδ13Crem
Δδ13C

Figure 4. Vertical profiles of globally horizontally averaged ocean DIC (top left) and δ^{13}C (bottom left) at years 0 (black) and 2500 (red) of experiment FW0.15. Right panels show changes (year 2500 minus year 0) in $\mathrm{DIC} = \mathrm{DIC}_{\mathrm{pre}} + \mathrm{DIC}_{\mathrm{rem}}$ and $\delta^{13}\mathrm{C} = \delta^{13}\mathrm{C}_{\mathrm{pre}} + \delta^{13}\mathrm{C}_{\mathrm{rem}}$ (green) as well as individual components preformed $\mathrm{DIC}_{\mathrm{pre}}$ and remineralized $\mathrm{DIC}_{\mathrm{rem}} = \mathrm{DIC}_{\mathrm{org}} + \mathrm{DIC}_{\mathrm{CaCO_3}}$. See Schmittner et al. (2013) for the calculation of the individual terms. The differences between the blue and green lines are due to changes in preformed DIC and δ^{13}C.

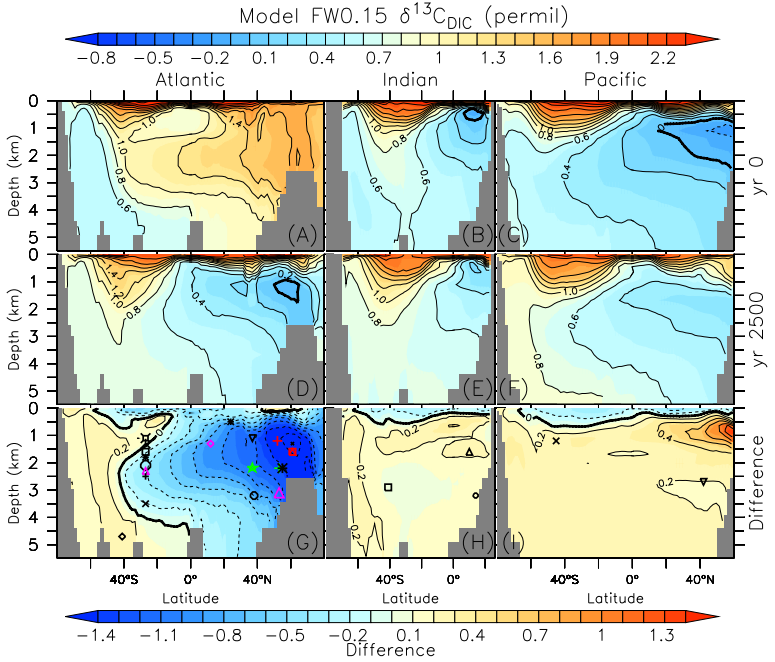
Model FW0.15 δ13CDIC (permil)
−0.8 −0.5 −0.2 0.1 0.4 0.7 1 1.3 1.6 1.9 2.2
Atlantic
Indian
Pacific
Depth (km)
yr 0
yr 2500
Difference
(A)
(B)
(C)
(D)
(E)
(F)
(G)
(H)
(I)
40°S
0°
40°N
Latitude
−1.4 −1.1 −0.8 −0.5 −0.2 0.1 0.4 0.7 1 1.3
Difference

Figure 5. Zonally averaged distributions of $\delta^{13}C_{DIC}$ (color shading and black isolines) as a function of latitude and depth simulated by model FW0.15 in the Atlantic (left), Indian (center) and Pacific (right) ocean basins at model years 0 **(A–C)** and 2500 (**D–F**; **A–F** use top color scale), and the difference (**G–I**; bottom color scale). Symbols in bottom panels denote locations of observations shown in Fig. 7.

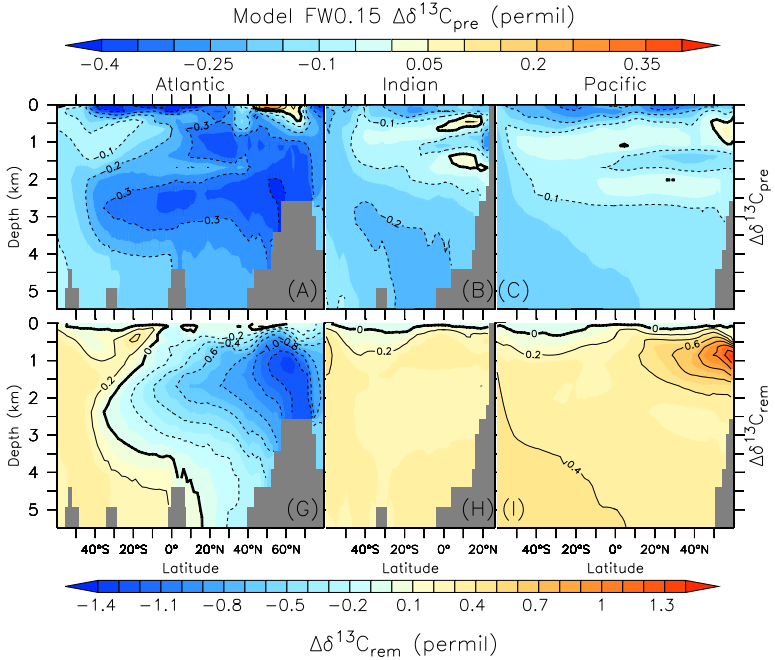
Model FW0.15 Δδ13Cpre (permil)
−0.4
−0.25
−0.1
0.05
0.2
0.35
Atlantic
Indian
Pacific
Depth (km)
Δδ13Cpre
(A)
(B)
(C)
(G)
(H)
(I)
40°S 20°S 0° 20°N 40°N 60°N
Latitude
−1.4 −1.1 −0.8 −0.5 −0.2 0.1 0.4 0.7 1 1.3
Δδ13Crem (permil)

Figure 6. Impact of AMOC collapse on $\delta^{13}C_{pre}$ (top) and $\Delta\delta^{13}C_{rem}$ (bottom). Zonally averaged changes between year 2500 and year 0 of model run FW0.15 in the Atlantic (left), Indian Ocean (center), and Pacific (right). Note the different color scales and isoline differences used. For absolute values of $\delta^{13}C_{pre}$ and $\Delta\delta^{13}C_{rem}$ see Figs. 6 and 12 in Schmittner et al. (2013).

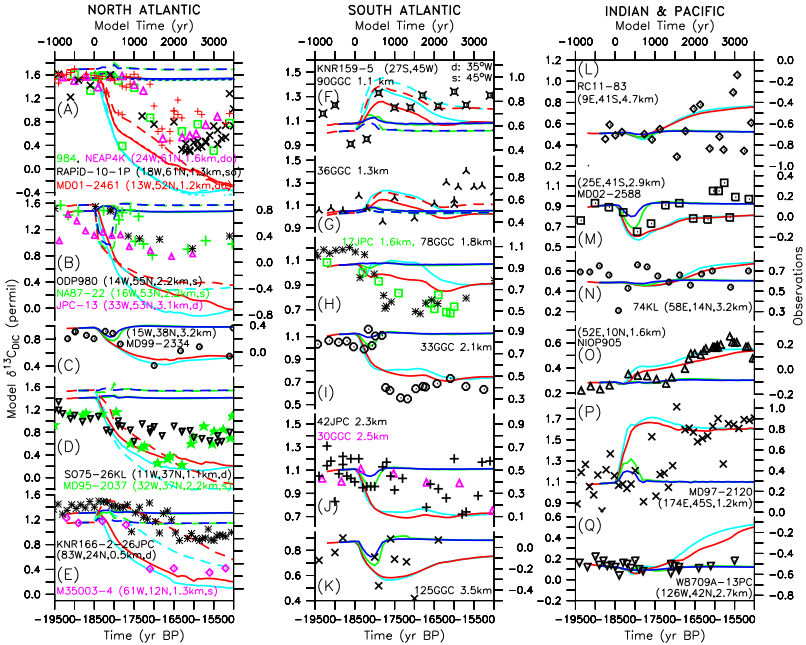
NORTH ATLANTIC
Model Time (yr)
SOUTH ATLANTIC
Model Time (yr)
INDIAN & PACIFIC
Model Time (yr)
Model δ13CDIC (permil)
Observations
Time (yr BP)
Time (yr BP)
Time (yr BP)
(A)
984, NEAP4K (24W,61N,1.6km,dot)
RAPID-10-1P (18W,61N,1.3km,sc)
MD01-2461 (13W,52N,1.2km,dot)
(B)
ODP980 (14W,55N,2.2km,s)
NA87-22 (16W,53N,2.2km,s)
JPC-13 (33W,53N,3.1km,d)
(C)
(15W,38N,3.2km)
MD99-2334
(D)
SO75-26KL (11W,37N,1.1km,d)
MD95-2037 (32W,37N,2.2km,s)
(E)
KNR166-2-26JPC
(83W,24N,0.5km,d)
M35003-4 (61W,12N,1.3km,s)
KNR159-5 (27S,45W) d: 35°W s: 45°W
90GGC 1.1 km
(F)
36GGC 1.3km
(G)
17JPC 1.6km, 78GGC 1.8km
(H)
33GGC 2.1km
(I)
42JPC 2.3km
30GGC 2.5km
(J)
(K)
125GGC 3.5km
(L)
RC11-83
(9E,41S,4.7km)
(25E,41S,2.9km)
MD02-2588
(M)
(N)
74KL (58E,14N,3.2km)
(52E,10N,1.6km)
NIOP905
(O)
(P)
MD97-2120
(174E,45S,1.2km)
(Q)
WB709A-13PC
(126W,42N,2.7km)

Figure 7. Comparison of simulated (lines as in Fig. 1; left and top axes) and observed (symbols as in Fig. 5; right and bottom axes) $\delta^{13}C_{DIC}$ timeseries in the North Atlantic **(A–E)**, South Atlantic **(F–L)**, Indian **(M–O)**, and Pacific **(P)** oceans. If no numbers are given on the right axis the scale is identical to the left axis. If numbers are given on the right axis the scale is different but the range (max–min) is identical to that of the left axis. Note that different ranges of the vertical axis are used for the different columns, whereas within each column they are similar.

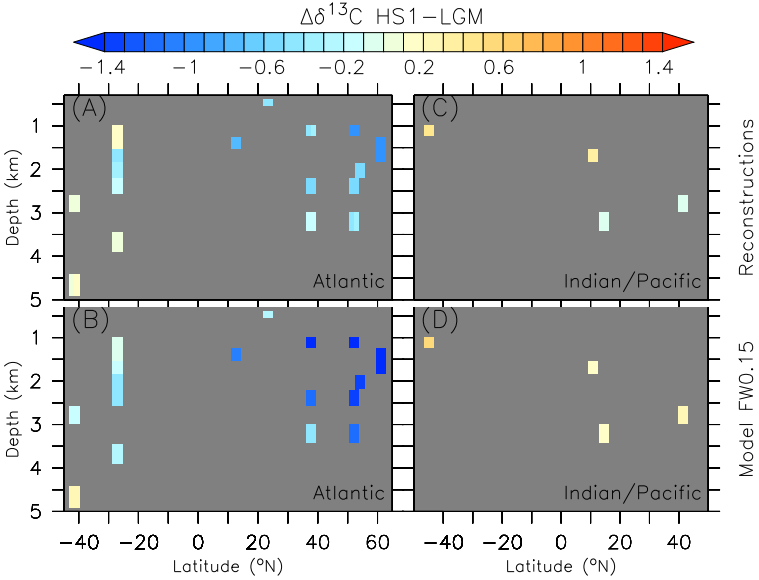
Δδ13C HS1−LGM
−1.4
−1
−0.6
−0.2
0.2
0.6
1
1.4
(A)
(B)
(C)
(D)
Atlantic
Indian/Pacific
Depth (km)
Latitude (°N)
Reconstructions
Model FW0.15

Figure 8. Heinrich Stadial 1 (16.5–15.5 ka BP) minus LGM (19.5–18.5 ka BP) difference in $\delta^{13}C_{DIC}$ in the Atlantic (left) and Indian and Pacific (right) basins from our high-resolution synthesis of reconstructions averaged on the model grid (top) compared to model FW0.15 results (bottom; averages of model years 2000 to 3000 minus averages of model years −1000 to 0.).

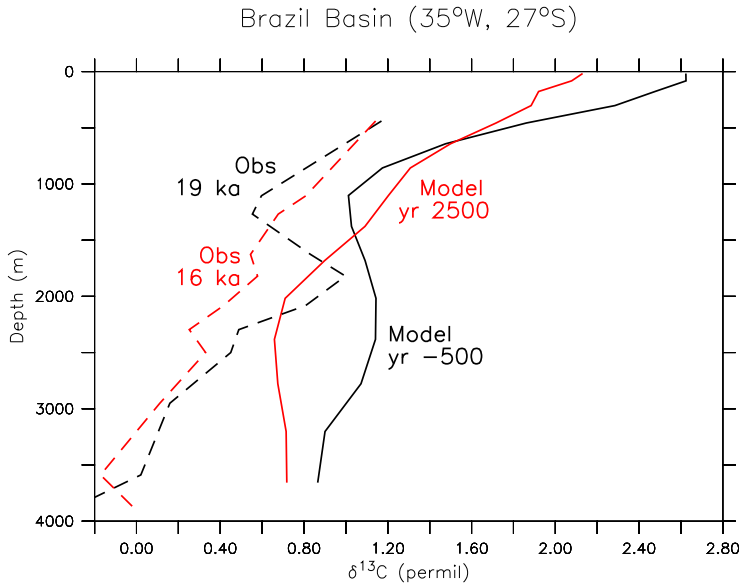
Brazil Basin (35°W, 27°S)
Depth (m)
0
1000
2000
3000
4000
0.00
0.40
0.80
1.20
1.60
2.00
2.40
2.80
δ13C (permil)
Obs
19 ka
Obs
16 ka
Model
yr 2500
Model
yr −500

Figure 9. Simulated (solid; model FW0.15) and observed (dashed) vertical profiles of $\delta^{13}C_{DIC}$ at the Brazil Margin in the South Atlantic before (black) and after (red) the AMOC collapse. Observations show 1 ka averages of smoothed (2 ka) data. Results for model FW0.2 are very similar to FW0.15 (not shown). However, models FW0.05 and FW0.1 show almost no changes from their initial (yr -500) distribution (not shown).

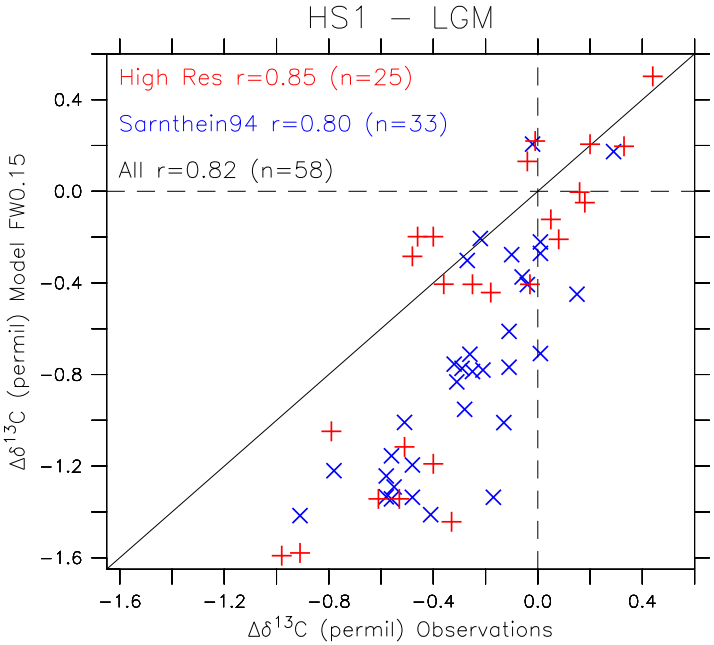
HS1 − LGM
High Res r=0.85 (n=25)
Sarnthein94 r=0.80 (n=33)
All r=0.82 (n=58)
0.4
0.0
−0.4
−0.8
−1.2
−1.6
Δδ13C (permil) Model FW0.15
−1.6
−1.2
−0.8
−0.4
0.0
0.4
Δδ13C (permil) Observations

Figure 10. HS1 minus LGM change in δ^{13}C from ref (Sarnthein et al., 1994; blue) our high-resolution compilation (red) vs. changes between years -500 and 2500 (1000 year centered averages) predicted by model experiment FW0.15 at the same locations. The diagonal $1:1$ line corresponds to a perfect match.

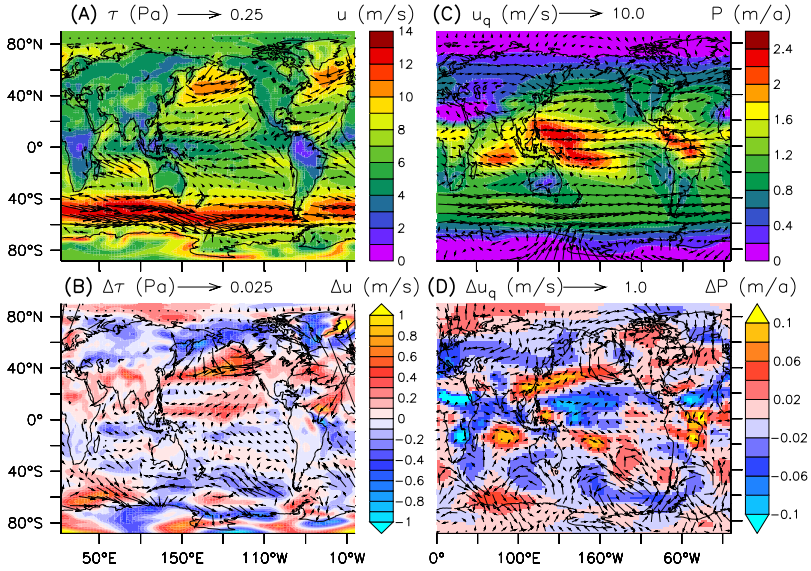
(A) τ (Pa) ⟶ 0.25
u (m/s)
(C) u_q (m/s) ⟶ 10.0
P (m/a)
(B) Δτ (Pa) ⟶ 0.025
Δu (m/s)
(D) Δu_q (m/s) ⟶ 1.0
ΔP (m/a)
80°N
40°N
0°
40°S
80°S
50°E
150°E
110°W
10°W
0°
100°E
160°W
60°W

Figure 11. (A) Annual mean wind stress τ (arrows) and wind speed u (color) fields used in the control run of the UVic model. **(B)** Changes in annual mean wind stress $\Delta\tau$ and wind speed Δu derived from a hosing simulation with the OSUVic model. **(C)** and **(D)** as **(A)** and **(B)** but for moisture advection velocities u_{q} (arrows) and precipitation (color). Note the differences in scales between the top and bottom panels.

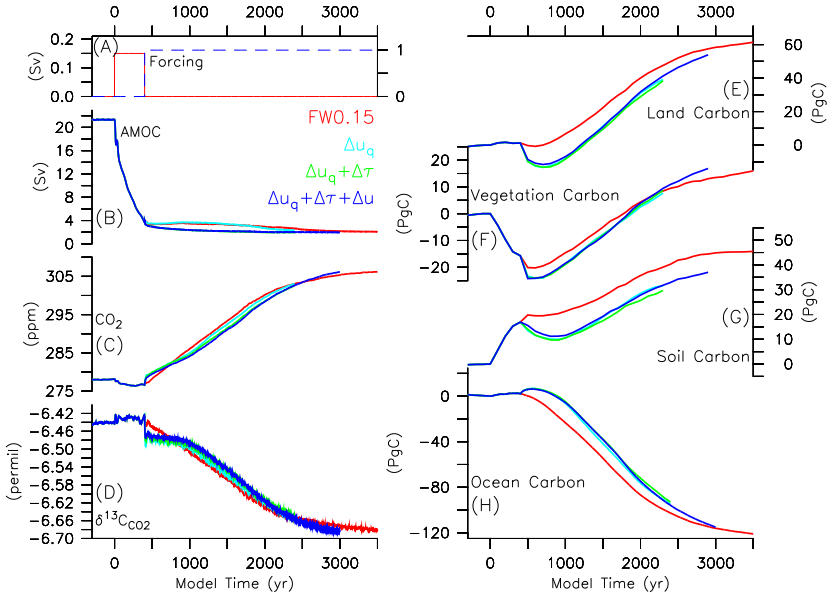
(A)
Forcing
(Sv)
FW0.15
Δu_q
$\Delta u_q+\Delta\tau$
$\Delta u_q+\Delta\tau+\Delta u$
AMOC
(B)
(C)
CO_2
(ppm)
(D)
$\delta^{13}C_{CO2}$
(permil)
Model Time (yr)
(E)
Land Carbon
(PgC)
Vegetation Carbon
(F)
(G)
Soil Carbon
Ocean Carbon
(H)
Model Time (yr)

Figure 12. Sensitivity to changes in winds. Experiment FW0.15 (red) is repeated with changes in moisture advection velocities u_{q} (light blue), u_{q} plus wind stress τ (green), and $u_{\mathrm{q}} + \tau$ plus wind speed u (dark blue) calculated from the OSUVic model. See Fig. 11 and text for more details.

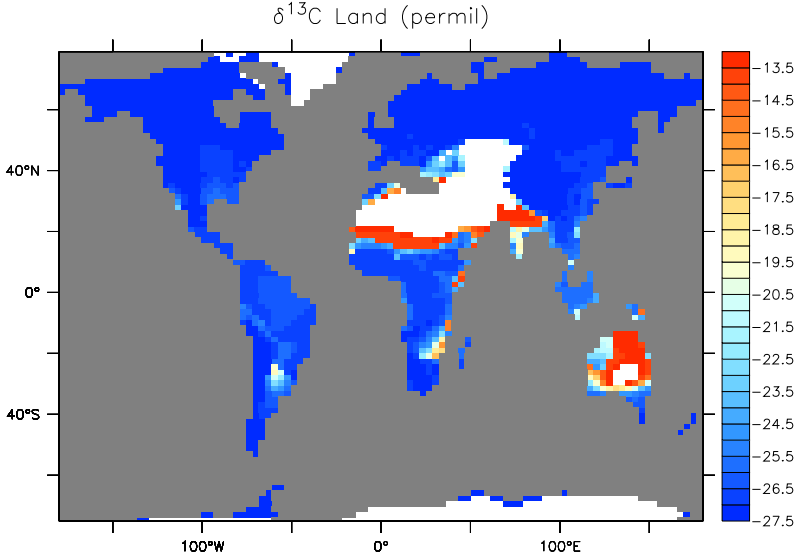
δ13C Land (permil)
40°N
0°
40°S
100°W
0°
100°E
13.5
14.5
15.5
16.5
17.5
18.5
19.5
20.5
21.5
22.5
23.5
24.5
25.5
26.5
27.5

Figure 13. Simulated average pre-industrial land δ^{13}C distribution (model year 0). Each pool's (five vegetation plant functional types, PFTs, and one soil, S, carbon compartment) δ^{13}C value was weighted by its mass in calculating the average as explained in figure caption 2. Desert regions with negligible vegetation carbon ($< 10\,\mathrm{g\,m^{-2}}$) are shown in white.